





Room temperature Mott metal–insulator transition in V_2O_3 compounds induced via strain-engineering

Cite as: APL Mater. 9, 021116 (2021); <https://doi.org/10.1063/5.0035865>

Submitted: 31 October 2020 . Accepted: 20 January 2021 . Published Online: 16 February 2021

 P. Homm,  M. Menghini,  J. W. Seo, S. Peters, and  J. -P. Locquet



View Online



Export Citation



CrossMark

ARTICLES YOU MAY BE INTERESTED IN

[Tuning metal-insulator transitions in epitaxial \$V_2O_3\$ thin films](#)

Applied Physics Letters **112**, 161902 (2018); <https://doi.org/10.1063/1.5023180>

[A physical method for investigating defect chemistry in solid metal oxides](#)

APL Materials **9**, 011106 (2021); <https://doi.org/10.1063/5.0033891>

[Progress and future prospects of negative capacitance electronics: A materials perspective](#)

APL Materials **9**, 020902 (2021); <https://doi.org/10.1063/5.0032954>



AIP Publishing HORIZONS

APL Materials

Materials Challenges for Memory · April 11-13, 2021 | Virtual Conference

Register Today!

Room temperature Mott metal-insulator transition in V_2O_3 compounds induced via strain-engineering

Cite as: APL Mater. 9, 021116 (2021); doi: 10.1063/5.0035865

Submitted: 31 October 2020 • Accepted: 20 January 2021 •

Published Online: 16 February 2021



View Online



Export Citation



CrossMark

P. Homm,¹  M. Menghini,^{1,2,a)}  J. W. Seo,³  S. Peters,⁴ and J. -P. Locquet^{1,b)} 

AFFILIATIONS

¹Department of Physics and Astronomy, KU Leuven, Celestijnenlaan 200D, 3001 Leuven, Belgium

²IMDEA Nanociencia, Cantoblanco, E-28049 Madrid, Spain

³Department of Materials Engineering, KU Leuven, Kasteelpark Arenberg 44, 3001 Leuven, Belgium

⁴SENTECH Instruments GmbH, Schwarzschildstr. 2, 12489 Berlin, Germany

^{a)}Author to whom correspondence should be addressed: mariela.menghini@imdea.org

^{b)}Electronic mail: jeanpierre.locquet@kuleuven.be

ABSTRACT

Vanadium sesquioxide (V_2O_3) is an archetypal Mott insulator in which the atomic positions and electron correlations change as temperature, pressure, and doping are varied, giving rise to different structural, magnetic, or electronic phase transitions. Remarkably, the isostructural Mott transition in Cr-doped V_2O_3 between paramagnetic metallic and insulating phase observed in bulk has been elusive in thin film compounds so far. Here, via continuous lattice deformations induced by heteroepitaxy, we demonstrate a room temperature Mott metal-insulator transition in 1.5% Cr-doped and pure V_2O_3 thin films. By means of a controlled epitaxial strain, not only the structure but also the intrinsic electronic and optical properties of the thin films are stabilized at different intermediate states between the metallic and insulating phases, inaccessible in bulk materials. This leads to films with unique features such as a colossal change in room temperature resistivity ($\Delta R/R$ up to 100 000%) and a broad range of optical constant values as consequence of a strain-modulated bandgap. We propose a new phase diagram for pure and Cr-doped V_2O_3 thin films with the engineered in-plane lattice constant as a tunable parameter. Our results demonstrate that controlling phase transitions in correlated systems by epitaxial strain offers a radical new approach to create the next generation of Mott devices.

© 2021 Author(s). All article content, except where otherwise noted, is licensed under a Creative Commons Attribution (CC BY) license (<http://creativecommons.org/licenses/by/4.0/>). <https://doi.org/10.1063/5.0035865>

I. INTRODUCTION

Vanadium sesquioxide (V_2O_3) is an example of a Mott insulator presenting both non-isostructural and isostructural metal-insulator transitions (MIT) as a function of temperature, doping, and pressure¹⁻³ and has attracted great interest for applications. V_2O_3 undergoes a non-isostructural MIT at 160 K upon cooling from a corundum paramagnetic metallic (PM) phase to a monoclinic antiferromagnetic insulating (AFI) phase,^{4,5} yielding a resistivity change of seven orders of magnitude.¹ In contrast to this low-temperature MIT, the isostructural Mott MIT between paramagnetic metallic (PM) and insulating (PI) phases occurs close to

room temperature (RT) and has been observed for a limited range of Cr doping (0.5%–1.7%) concentration.⁶ This transition has been observed in bulk crystals with a resistivity change of three orders of magnitude and a variation in a -axis lattice parameter of 1% within the same corundum structure.^{1,2}

The bulk phase diagram of V_2O_3 as a function of temperature, doping, and applied pressure has been well established based on extensive experimental data from single crystals⁷⁻¹⁰ and supported by a number of theoretical calculations that successfully predicted the density of states (DOS) of the different phases.¹¹⁻¹³ In thin films, various deviations from the bulk phase diagram have been observed. For example,

recently, it has been shown that the AFI phase in thin films is characterized by stripe domains related to different lattice distortions.¹⁴ Then, the low-temperature PM-AFI transition has been reported by many groups,⁶ while the isostructural RT Mott transition involving PM-PI phases—despite greater interest for applications—has been missing in most studies.^{6,15,16} This suppression of the RT MIT has been attributed to the clamping effect of the substrate in epitaxial films¹⁶ or to structural disorder and small grain size present in polycrystalline films.^{6,15} Especially, epitaxial strain has so far shown its strong effect on the phase transitions in the vanadate family, which can range from a change in transition temperature¹⁷ or direction dependent electrical properties¹⁸ in VO₂ films to a complete suppression of the low-temperature phase transition¹⁹ in V₂O₃ films.

Salev *et al.*²⁰ demonstrated that the low-temperature MIT can actively be modulated through a voltage-actuated PMN-PT [Pb(Mg,Nb)O₃-PbTiO₃] ferroelectric actuator, which transfers switchable ferroelastic strain into the epitaxial V₂O₃ film and leads to a giant nonvolatile resistive switching of 1000%, while the effect at room temperature is only $\Delta R/R \sim 18\%$. Querré *et al.*²¹ observed non-volatile resistive switching in Cr-doped V₂O₃ films, where conducting filaments form as a result of a local electric field driven low-temperature Mott transition. These recent achievements have pointed out the great potential of Mott insulator thin films with large resistivity changes across phase transitions for application in sensors and memory devices. However, triggering the metal-insulator phase transition at room temperature would be even more desirable for their implementation in devices.

The RT MIT has been observed in polycrystalline thin films of Cr-doped V₂O₃ by optical transmission measurements, while electrical resistivity did not show a transition.⁶ Epitaxial V₂O₃ thin films showed a local pressure-induced transition at RT by means of a contact AFM tip,²² whereas a systematic study by varying the oxygen doping concentration in epitaxial films did not show the RT MIT.²³ These results indicate that the RT MIT can be stabilized within a narrow window of conditions, which need to be systematically explored. So far, a generalized phase diagram for V₂O₃ thin films does not exist but would be highly desirable to gain fundamental understanding about the interplay between epitaxial strain and Mott transition and to use these films in practical applications.

Here, we present a systematic strain-engineering study of 1.5% Cr-doped and pure V₂O₃ thin films. Our approach is based on the use of precisely engineered oxide heterostructures as artificial substrates to systematically tune the in-plane lattice parameter in the pure and 1.5% Cr-doped V₂O₃ thin films within and beyond the reported structural states in the bulk. The in-plane lattice parameters of the engineered substrates were gradually adjusted between 4.943 Å and 5.037 Å by varying the precise composition of the thin film buffer layer. Detailed chemical analysis by means of Energy Dispersive X-ray (EDX) spectroscopy confirmed the chemical composition of the buffer layers and the V₂O₃ films. Extensive structural studies including High Resolution X-Ray Diffraction (HRXRD), Reciprocal Space Maps (RSMs), and High Resolution Transmission Electron Microscopy (HRTEM) revealed the in-plane lattice parameters of the heterostructures and the amount of induced stress. Temperature-dependent electrical resistivity curves were measured using the van der Pauw (VDP) configuration. In addition, optical properties were addressed by Spectroscopic Ellipsometry (SE) to

illustrate how physical properties in the V₂O₃ thin films can be fully controlled by epitaxial strain.

The results show an effective transfer of strain achieved by heteroepitaxy leading to a Mott MIT in a wide range of temperatures around RT in 1.5% Cr-doped and pure V₂O₃ compounds. We observed a colossal change in room temperature resistivity (RTR) with $\Delta R/R$ up to $\sim 100\,000\%$ as well as a significant change in optical constants associated with the strain-modulated bandgap of these Mott insulators. Based on these results, a novel phase diagram of V₂O₃ thin films was proposed with the RT in-plane parameter as a variable. These results demonstrate that meticulous strain engineering is a powerful tool to tune physical properties of strongly correlated electron systems and also allows accessing novel states unaccessible in bulk. The stabilization and control of the MIT at RT in 1.5% Cr-doped and pure V₂O₃ thin films is an important achievement toward the implementation of Mott materials in devices.

II. EXPERIMENTAL

A. Thin film growth

All the thin film layers were deposited on (0001)-Al₂O₃ substrates by oxygen-assisted molecular beam epitaxy (MBE). The vacuum chamber had a base pressure of 10^{-9} Torr, and it was equipped with RHEED to confirm the epitaxial growth *in situ*. The oxide heterostructures consist of a 40 nm Cr₂O₃ epitaxial layer followed by a 30 nm thick (Cr_{1-y}Fe_y)₂O₃ solid solution ($y = 0$ corresponds to a 40 nm Cr₂O₃ only). To guarantee that all V₂O₃ film compounds have the same chemical interface with the heterostructure, an ultrathin 3 nm Cr₂O₃ layer was deposited on the (Cr_{1-y}Fe_y)₂O₃ alloys with $y > 0$. Finally, the 60 nm 1.5% Cr-doped and pure V₂O₃ films were deposited on the artificial substrates composed by the oxide heterostructures.

B. Structural characterization

The structural properties of the samples were characterized by means of high-resolution x-ray diffraction (XRD) with a Panalytical X'pert Pro diffractometer using monochromatic K α_1 radiation of a Cu anode. Out-of-plane measurements in the $\theta/2\theta$ configuration were done around the symmetric peak (0006) and two-axis measurements—reciprocal space maps (RSM)—around the asymmetric peak (1 0 $\bar{1}$ 10) were performed to extract in-plane and out-of-plane lattice spacings. Besides, the structural quality and composition were also addressed by transmission electron microscopy (TEM) and energy dispersive x-ray spectroscopy (EDX), respectively. TEM and EDX analysis were performed using a probe-lens corrected JEOL ARM200F scanning transmission electron microscope operating at 200 kV and equipped with a cold-field emission gun and a Centurio energy dispersive x-ray spectrometer. The TEM samples were prepared by means of a focused ion beam (FIB).

C. Electrical and optical characterization

Temperature-dependent resistivity measurements in the VDP configuration were performed in an Oxford Optistat CF2-V cryostat using a Keithley 4200-SCS parameter analyzer. The temperature sweep rate was of 1 K per minute. Finally, SE measurements from 70 meV to 0.5 eV in the MIR and from 0.5 eV (NIR) to 6 eV (UV)

were performed at SENTECH Instruments GmbH in Berlin with a SENDIRA and SENresearch 4.0 SER 850 DUV ellipsometers, respectively. The ellipsometer angles ψ and Δ were measured at room temperature using three different angles of incidence (65° , 70° , and 75°). Independent measurements on the layers in the oxide heterostructures were performed before the 1.5% Cr-doped and pure V_2O_3 films were deposited, and the data were fitted applying the Tauc-Lorentz oscillator model.⁵¹ Then, the measurements were repeated on the stack with the top 1.5% Cr-doped or pure V_2O_3 films and the data were fitted applying the same optical model used for analyzing the layers in the heterostructure.

III. RESULTS AND DISCUSSION

Systematic straining of 1.5% Cr-doped and pure V_2O_3 films was achieved by using oxide heterostructures consisting of several epitaxial thin films with the corundum structure. The thickness of the 1.5% Cr-doped and pure V_2O_3 layers was kept to 60 nm. As there is a large lattice mismatch of $>4\%$ between Al_2O_3 and Cr-doped and pure V_2O_3 ,¹⁶ a 40 nm buffer layer of Cr_2O_3 was first deposited. As demonstrated previously,²⁴ the Cr_2O_3 buffer layer can grow almost relaxed on Al_2O_3 and enables the subsequent growth of V_2O_3 structurally decoupled from the substrate with a lattice mismatch of about 0.1%.

In addition, Cr_2O_3 has the additional advantage that it can be alloyed with Fe. $(Cr_{1-y}Fe_y)_2O_3$ also forms a corundum structure with the in-plane lattice parameter that can be changed by more than 1% (between $a = 4.959 \text{ \AA}$ and $a = 5.035 \text{ \AA}$)²⁵ by varying the Fe content y . On top of this $(Cr_{1-y}Fe_y)_2O_3$ layer, an ultrathin Cr_2O_3 layer (3 nm) was deposited that remained coherent/pseudomorphic with the underlying $(Cr_{1-y}Fe_y)_2O_3$ layer. This ultrathin Cr_2O_3 layer ensured that the 1.5% Cr-doped and pure V_2O_3 films deposited on the buffer stack experienced exactly the same chemical interface so that possible chemical effects of the underlying layer can be excluded. Figure 1(e) shows a cross section EDX map obtained from a 1.5% Cr-doped V_2O_3 film grown on the buffer stack described above. The color code linked to different Cr concentrations in the layers reflects the layout of the final heterostructure used for this study. The Cr doping of 1.5% was specifically chosen to ensure the presence of a single PI phase at RT, while in pure V_2O_3 , a single PM phase is expected.^{1,2} This allows us to address the effect of strain engineering on both phases involved in the Mott transition.

The in-plane and out-of-plane lattice parameters of the strained (doped and undoped) V_2O_3 films were determined by means of extensive HRXRD analysis. Figures 1(a) and 1(b) show the RSMs of the 1.5% Cr-doped and pure V_2O_3 films, measured around the $(1\ 0\ \bar{1}\ 10)$ peak of each layer in the stacks. They clearly demonstrate that all layers in the stacks are single-phase and epitaxial and preserve the corundum structure. No secondary phases were detected. The excellent structural quality is evidenced by the presence of finite-size oscillations in out-of-plane $\theta/2\theta$ XRD measurements (see Fig. S1 of the supplementary material).

The $(1\ 0\ \bar{1}\ 10)$ peak positions of the $Cr_2O_3/(Cr_{1-y}Fe_y)_2O_3/Cr_2O_3$ stack—and the lattice parameters (a and c)—confirm that the engineered buffer has an in-plane lattice parameter effectively decoupled from the substrate. The blue and red dots in the RSMs in Figs. 1(a) and 1(b) mark the bulk lattice parameters of the PM and PI phases,

respectively. By increasing the Fe content in $(Cr_{1-y}Fe_y)_2O_3$, the lattice parameters a and c of the 1.5% Cr-doped and pure V_2O_3 films gradually move from the blue dot position (corresponding PM with a_{PM} , c_{PM}) to the red dot position (corresponding PI with a_{PI} , c_{PI}). For the Fe concentration of $y = 1$ (Fe_2O_3), the lattice parameters go even beyond the PI bulk value.

In-plane lattice parameters of the films are calculated based on the RSM data and summarized in Fig. 1(c) as a function of the Fe content y together with the corresponding values for the buffer layers. The data show that the 1.5% Cr-doped and pure V_2O_3 films roughly follow the in-plane lattice parameter evolution of the buffer layers. It is important to note that no systematic widening of the RSM peaks is observed as the Fe content changes (except for the cases with $y = 1$) in the buffer layers. Moreover, by using the Scherrer equation for the out-of-plane diffraction peaks, we found that the crystalline coherence is almost the same as the thickness extracted from x-ray reflectivity measurements (only an average difference of 3%), evidencing a good uniformity of the films lattice structure. These results indicate that the designed buffer layers are sufficient to grow films with a well-defined lattice constant across the whole film. In the case of $y = 1$, the observed RSM peak broadening could be due to local inhomogeneities or oxygen vacancies that can be more favorable due to the larger tensile strain in these films.

The in-plane lattice parameter of the $(Cr_{1-y}Fe_y)_2O_3$ layer (light-blue squares) increases linearly with y (only the data point for $y = 1$ deviates from this linear trend), evidencing that the produced buffer effectively tailors the amount of induced strain as a function of the Fe content. From the in-plane lattice parameters, the resulting in-plane strain was calculated as $\epsilon_{in-plane} = (a_{film} - a_{bulk})/a_{bulk}$, with a_{bulk} equal to a_{PI} (a_{PM}) for 1.5% Cr-doped (pure) V_2O_3 films. Figure 1(d) shows the evolution of the c/a ratio as a function of the strain in the Cr-doped (left) and pure (right) V_2O_3 films. The continuous decrease in c/a between the PM and PI bulk values (marked by blue and red line, respectively) with $\epsilon_{in-plane}$ indicates that the c -axis adjusts to the imposed in-plane deformations. The measured changes in the c/a ratio of our strained films slightly deviate from what is expected considering only an elastic deformation: The Poisson ratio for the PI phase in 1.5% Cr- V_2O_3 for $\epsilon_{in-plane} = -0.8$ yields $c/a = 2.831$,²⁶ while we find $c/a = 2.822$ experimentally. The most remarkable result is the continuous change in c/a between the PM and PI phases, in contrast to the discontinuous one observed in single crystals.² This deviation indicates that the bulk and thin films of doped and pure V_2O_3 behave differently, allowing us to explore states with intermediate lattice parameters that are not stable in bulk samples. As highlighted in Fig. 1(d), in pure V_2O_3 films only tensile strain is possible because the Cr_2O_3 layer has nearly the same in-plane lattice parameter as the PM phase, and alloying with Fe leads to larger in-plane parameters. On the contrary, both compressive and tensile strains are accessible for the 1.5% Cr-doped V_2O_3 films, which should be in the PI phase in the unstrained bulk phase.

Figure 1(e) shows a representative color-coded EDX map of the entire stack illustrating the sharp interfaces present across the different layers in the oxide heterostructure. Comparable results were obtained for 1.5% Cr-doped (pure) V_2O_3 films on the different buffers. In particular, systematic EDX line scans across the interface between the ultrathin 3 nm Cr_2O_3 layer and the 1.5% Cr-doped and pure V_2O_3 layers confirmed that there is no Cr diffusion into the top

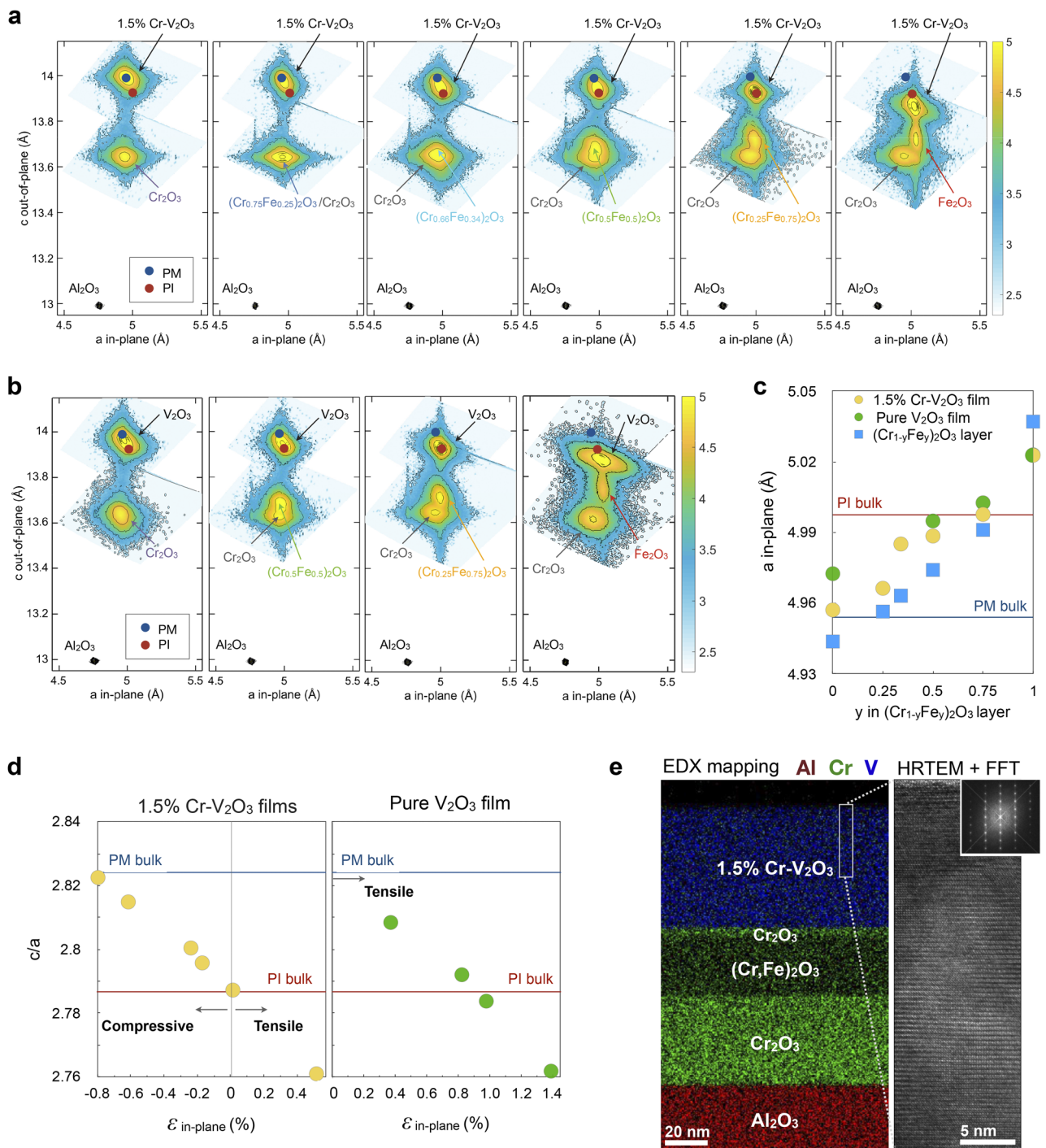


FIG. 1. Structural properties of strained 1.5% Cr-doped and pure V₂O₃ films. [(a) and (b)] RSMs around the (1 0 $\bar{1}$ 10) reflections transformed to in-plane and out-of-plane lattice spacings of the 1.5% Cr-doped and pure V₂O₃ films grown on the different (Cr_{1-y}Fe_y)₂O₃/Cr₂O₃ heterostructures. The PM and PI bulk lattice parameters are indicated by blue and red dots, respectively. (c) In-plane lattice parameters of the (Cr_{1-y}Fe_y)₂O₃ alloy layers in the oxide heterostructures (light blue squares) and the corresponding ones for the 1.5% Cr-doped (yellow circles) and pure (green circles) V₂O₃ films. (d) c/a ratio as a function of the in-plane strain ($\epsilon_{in-plane}$) induced by heteroepitaxy onto the 1.5% Cr-doped and pure V₂O₃ films. In (c) and (d), PM and PI bulk values are indicated by the blue and red lines, respectively. (e) Left: color-coded EDX mapping of a stack representative of the 1.5% Cr-doped V₂O₃ film series. Right: HRTEM image of the top layer and the corresponding Fast-Fourier Transform (FFT).

vanadium oxide layer. The Cr content in the Cr-doped films was estimated to be $1.5\% \pm 0.3\%$. Also the HRTEM image and corresponding Fast Fourier Transform (FFT, shown in the inset) demonstrate the single-crystalline character of the top layer across its whole thickness. The lattice spacings determined by HRTEM were in agreement with those extracted from HRXRD [Fig. 1(c)].

The temperature-dependent electrical resistivity curves $R(T)$ of the 1.5% Cr-doped and pure V_2O_3 films are shown in Figs. 2(a) and 2(b), respectively, along with the reference curves (gray dashed lines) originating from 1% Cr-doped and pure V_2O_3 single crystals.²⁷ Note that the $(Cr_{1-y}Fe_y)_2O_3$ layers are insulating in agreement with the bandgaps of 2.1 eV and 3.2 eV for (Fe_2O_3) and (Cr_2O_3) ,²⁸ respectively, and therefore, the transport measurements solely probe the V_2O_3 thin films.

The low temperature (LT) transition can be seen in all samples, except in those with the largest in-plane lattice parameter (red dotted curves in each figure), which correspond to the highest Fe content $y = 1$ in the $(Cr_{1-y}Fe_y)_2O_3$ buffer. The T_{MIT} (marked with star symbols in Figs. 2(a) and 2(b)) was determined from the inflection point in the $d\ln R(T)/dT$ curve and increased from 150 K to 180 K with the in-plane lattice parameter in both series. This is similar to the change in T_{MIT} upon Cr doping in bulk [see the change in T_{MIT} in the bulk 1.5% Cr-doped and pure V_2O_3 samples shown in Figs. 2(a) and 2(b)]. Nevertheless, there are differences between the strained films—at constant doping—and bulk samples as a function of doping, such as the lack of sharp transitions and significantly reduced resistance jumps at the transition temperature. These differences can be due to several reasons including the in-plane clamping of the film lattice parameters that hampers the structural phase transitions as well as small variations in composition such as Cr-doping and oxygen content. It has been previously reported that the increase in tensile strain²⁹ or oxygen deficiency³⁰ can cause an increase in RTR

and a decrease in the resistance ratio across the MIT. Therefore, possible formation of oxygen vacancies could explain the crossing of the $R(T)$ curve for the most strained films (red dotted curves) with the one of films with a smaller lattice parameter (yellow dotted curves).

The PM–PI transition close to RT is, as expected, completely absent in the 1.5% Cr-doped V_2O_3 films for all in-plane parameters, most probably due to the clamping effect.¹⁶ Nonetheless, a significant change in the RTR occurs when changing the in-plane lattice parameter of the films. This trend is also observed in the pure V_2O_3 thin film series [Fig. 2(b)]. Figure 2(c) highlights the RTR values as a function of the in-plane lattice parameter for both film series, which clearly shows a PM to PI transition triggered by epitaxial strain. The most striking result is that an in-plane lattice deformation of $\sim 1\%$ can trigger a $\Delta R/R$ as large as 100 000% in both the strained 1.5% Cr-doped (yellow circles) and the pure (green circles) V_2O_3 films. To our knowledge, this is the largest change in RTR achieved by epitaxial strain in V_2O_3 compounds.^{20,22,32}

The RTR of the 1.5% Cr-doped V_2O_3 film with the smallest in-plane lattice parameter ($a = 4.957 \text{ \AA}$) is closer to the bulk RTR value of the PM phase of pure V_2O_3 (marked by the gray cross $PM^{undoped}$) than to the one of the PM phase of 1% Cr-doped V_2O_3 compound (marked by the blue cross $PM^{1\%Cr}$). This low RTR value suggests that the metallic state achieved by strain in 1.5% Cr-doped V_2O_3 thin films is mostly determined by a collective modification of the crystal lattice and electronic band structure in contrast to bulk samples, where the non-perfectly homogeneous distribution of Cr dopants can lead to electron scattering and to higher RTR.

Optical studies have been invaluable for understanding the underlying physics in V_2O_3 systems^{7,34–38} because electron correlation effects appear as distinct signatures in the optical conductivity spectra of metallic and insulating phases and the Mott MIT is accompanied by large spectral weight changes.^{33,39} The optical

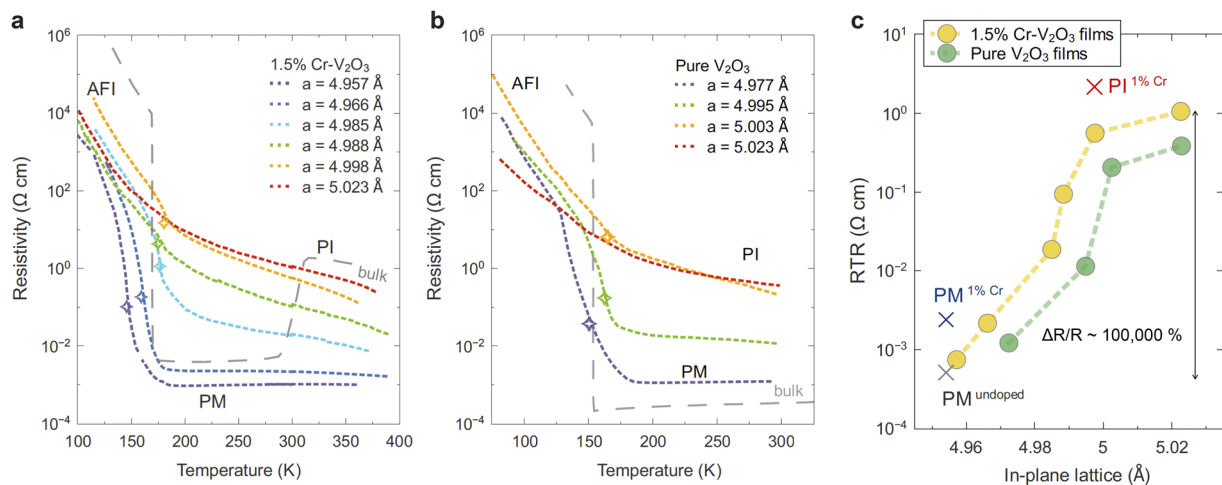


FIG. 2. Electrical properties of strained 1.5% Cr-doped and pure V_2O_3 films. [(a) and (b)] Resistivity curves $R(T)$ on cooling of the 1.5% Cr-doped and pure V_2O_3 films with different in-plane lattice parameters engineered by heteroepitaxy. T_{MIT} on cooling is indicated with a star symbol. The gray dashed line in (a) corresponds to a 1% Cr-doped V_2O_3 single crystal and in (b) to a V_2O_3 single crystal (both curves extracted from Ref. 27). (c) Room temperature resistivity (RTR) of the 1.5% Cr-doped and pure V_2O_3 films as a function of their in-plane lattice parameter. The blue and red crosses correspond to the values for a 1% Cr-doped V_2O_3 single crystal in the PM and PI phases, respectively, and the gray cross to the pure V_2O_3 one. Bulk values taken from Ref. 27 and Ref. 31.

conductivity spectra are shown in Fig. 3(a) for the strained 1.5% Cr-doped (top) and pure (bottom) V_2O_3 films. The features [labeled from (i) to (iv)] are assigned to the optical transitions depicted in Fig. 3(b). The scheme in Fig. 3(b) shows the DOS of metallic (PM) and insulating (PI) phases based on the one-band Hubbard model³³ in which the vanadium $3d$ band is composed of the quasiparticle peak (QP) around the Fermi level in the PM phase, defining feature (i) and the incoherent bands [so-called Low Hubbard Band (LHB) and Upper Hubbard Band (UHB)] emerging at $E - E_F = \pm U/2$, each of width W and separated by the Coulomb energy U . Note that the energy scale of the optical transitions (ii) and (iii) is in the orders of $U/2$ and U , respectively, and the Mott gap in the insulating state is in the order of $\Delta^* = U - W$.

Although in the case of V_2O_3 , the realistic multi-orbital scenario of the V $3d$ bands (i.e., Hubbard bands and QP are composed of two different orbitals) makes the DOS and optical transitions much more complex,^{36,40} the optical responses across the Mott MIT can be explained semiquantitatively based on the one-band Hubbard model for the optical conductivity.³³ The real part of the optical conductivity σ_1 , defined as $\sigma_1(\omega) = 2\varepsilon_0nk$, with ω being the angular frequency and ε_0 being the vacuum permittivity,⁴¹ has been calculated

from the optical constants (index of refraction, n , and extinction coefficient, k) derived by Spectroscopic Ellipsometry (SE) experiments performed at RT in an energy range from 0.5 eV to 6 eV (see the [supplementary material](#) for details).

Consistent with the one-band Hubbard model,³³ a signature of the Drude conductivity [feature (i), associated with optical transitions within the quasiparticle (QP) peak in the PM phase] is spotted at low energies in both film series with the smallest in-plane lattice parameters. The effects of electron correlation appear in the visible range as features (ii) (~ 1.4 eV in film spectra) and (iii) (~ 2.8 eV in film spectra), associated with optical transitions between the QP peak and the Hubbard bands and between LHB and UHB, respectively. Finally, the peak around 4 eV [labeled (iv)] observed in all films is related to transitions from the oxygen $2p$ bands.

As shown in Fig. 3(a), the features below 2 eV [(i) and (ii)] in σ_1 significantly decrease, when moving from the PM to the PI state triggered by epitaxial strain, owing to the spectral weight transferred between the Hubbard bands and the QP. The drastic decrease in σ_1 in this low energy range for the insulating films is directly related to the suppression of the QP and suggests the gradual opening of a gap across the Mott MIT in both strained V_2O_3 thin film series.

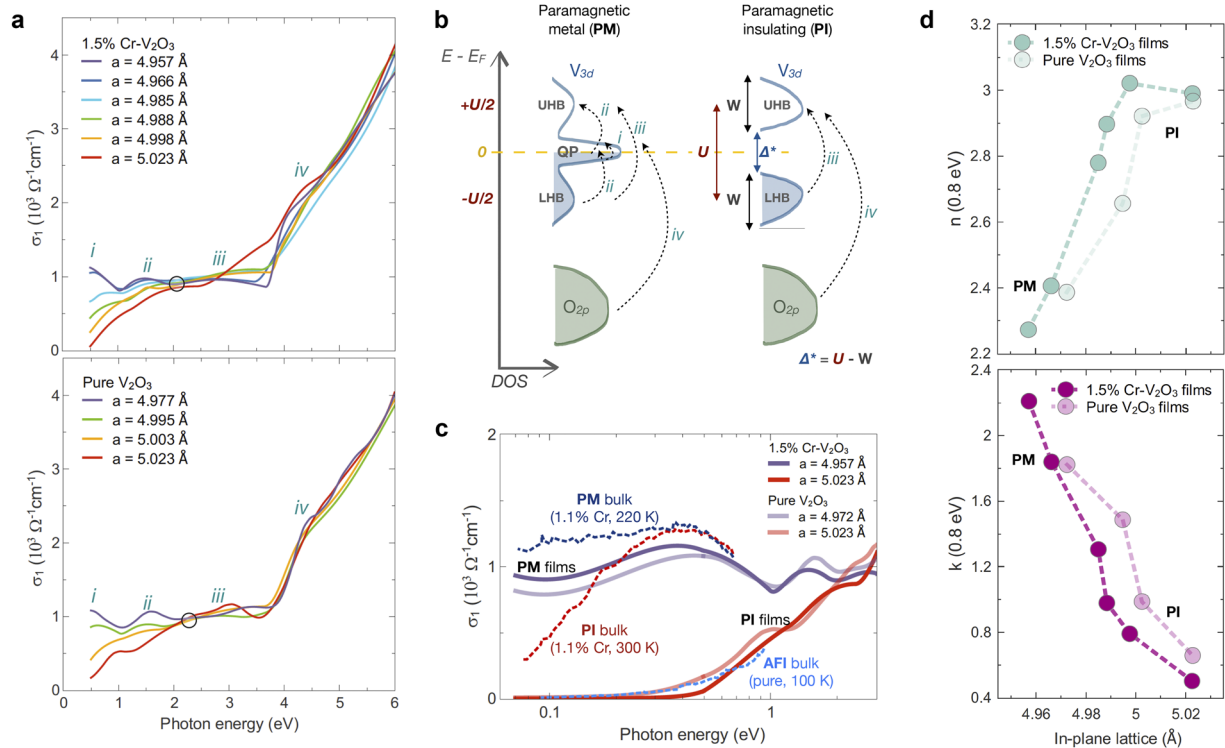


FIG. 3. Spectral optical properties of strained 1.5% Cr-doped and pure V_2O_3 thin films. (a) Real part of the optical conductivity (σ_1) as a function of the photon energy of the strained 1.5% Cr-doped (top) and pure V_2O_3 (bottom) thin film series. Interband transitions are labeled (i)–(iv) according to schematics in (b). The circles indicate isosbestic points at around 2.1 eV in both series. (b) Sketch of the electronic density of states (DOS) and optical excitations in the PM and PI phases of V_2O_3 compounds based on the model for the optical conductivity in Mott–Hubbard systems.³³ (c) Optical conductivity curves extended down to 70 meV in the mid-infrared (MIR) for the films with the extreme in-plane lattice parameters of each series. The dark blue dashed and red curves correspond to the PM and PI spectra of a 1.1% Cr- V_2O_3 single crystal, and the light blue one correspond to the AFI spectrum of a pure V_2O_3 single crystal. Bulk data taken from Refs. 7 and 34. (d) Optical constants n (top) and k (bottom) at the photon energy of 0.8 eV ($\lambda = 1550$ nm) of each series as a function of the engineered in-plane lattice parameter.

The data in Fig. 3(a) also reveal isosbestic points near 2.1 eV in both series (marked by circles). Such a point is a characteristic feature of Mott transitions,⁴² which has been observed in V_2O_3 thin films, single crystals,^{36,37} and VO_2 films^{38,43} but for temperature-dependent optical conductivity spectra, which intersect at the same σ_1 and energy values due to redistributions of spectral weight associated with a change from itinerant to localized electrons. Consequently, the presence of an isosbestic point in the RT optical conductivity spectra of both strained film series further suggests that a Mott phase transition can be triggered by continuous lattice deformation induced by heteroepitaxy.

In Fig. 3(c), the optical conductivity spectra extended down to the mid-infrared (MIR) regime of the 1.5% Cr-doped and pure V_2O_3 films with the smallest and largest in-plane lattice parameters are shown. For comparison, the optical conductivity curves obtained from single crystals [1.1% Cr-doped V_2O_3 single crystal in the PM (220 K) and PI (300 K) phases and pure V_2O_3 single crystal in the AFI (100 K) phase]^{7,34} are added. These bulk data illustrate that there is only a small drop in spectral weight below 1 eV linked to the opening of a bandgap of ~ 0.12 eV– 0.2 eV⁴⁴ for the Mott PM–PI transition in bulk. In contrast, the changes in the strained films are spectacular with a significant spectral weight drop and opening of a much larger bandgap of up to ~ 0.5 eV. There has been no comparable precedent report in the literature. The gradual decrease in σ_1 for energies below 1 eV as the lattice parameter increases, and the films become more insulating, indicates that the large spectral weight at low energies might not be an intrinsic property of the PI phase. In addition, it is remarkable that the evolution of σ_1 of the more insulating films resembles that of the reference V_2O_3 single crystals in the AFI phase, for which a large bandgap of 0.6 eV opens.⁴⁵ Our optical data [features (ii) and (iii)] indicate that U in the films is of the same order as in bulk. Therefore, a bandwidth reduction as a function of a -axis expansion is possibly the origin of the larger gap in the PI phase in films with $a > 4.985$ Å, as the Mott gap is $\Delta^* = U - W$.

The modulation of the bandgap, associated with intermediate states stabilized across the Mott transition, allows a considerable range of tuning of the optical constants at RT. For example, Fig. 3(d) displays the optical constants n (top) and k (bottom) at the photon energy of 0.8 eV—which corresponds to a wavelength of 1550 nm typically used in telecommunications—across the Mott transition at RT in both series. At this photon energy, n varies between ~ 2.3 and ~ 3 , while k changes between ~ 2.2 and ~ 0.5 as a function of the in-plane lattice parameter. These trends and values are similar to those reported for the temperature driven MIT in VO_2 ;^{43,46} however, the transition in the latter occurs at about 70°C , whereas our films show a transition at RT, which is beneficial for device applications. It also has to be noted that the optical constants for V_2O_3 compounds have not been reported previously. For example, the n and k values of the 1.5% Cr-doped V_2O_3 films in the whole NIR–UV energy range can be found in Fig. S2.4 of the [supplementary material](#).

The structural, electrical, and optical results reported here for pure and Cr-doped V_2O_3 thin films indicate that the well-known temperature–doping phase diagram [see Fig. 4 (top)]—for bulk V_2O_3 cannot be used to represent the different phases achieved via strain engineering. Figure 4 (bottom) shows the proposed phase diagram where temperature and in-plane lattice parameter are the variable axes. The absence of a PM–PI phase transition with

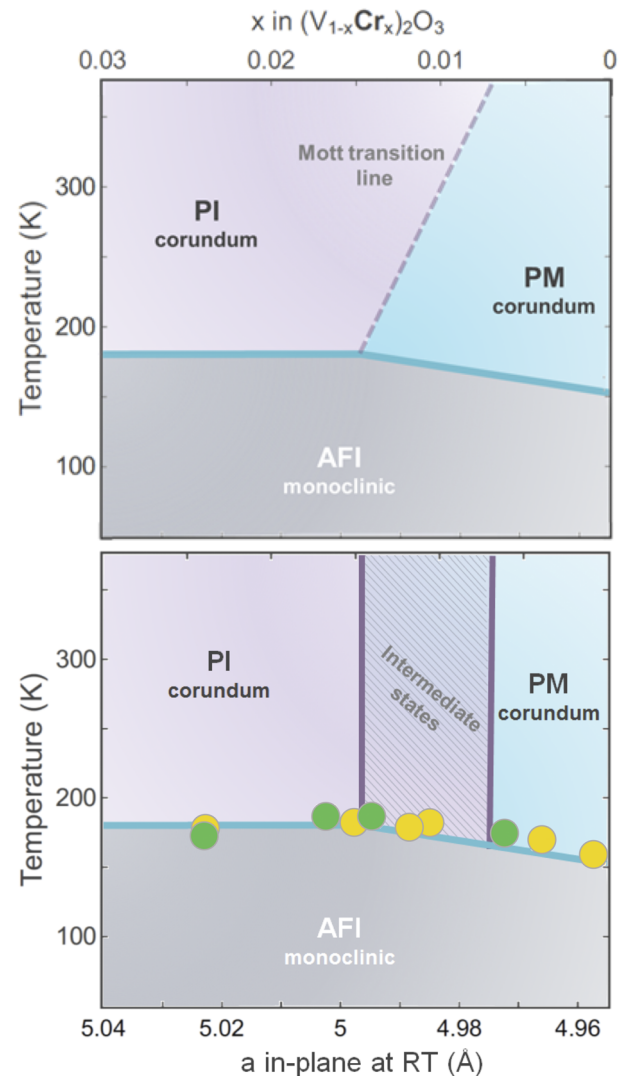


FIG. 4. Top: temperature–Cr-doping phase diagram of bulk V_2O_3 (adapted from Ref. 1) The dotted line corresponds to the Mott PM–PI transition and the continuous line corresponds to the LT transition to the AFI phase. Bottom: proposed temperature–in-plane lattice parameter (an in-plane at RT) phase diagram for pure and Cr-doped V_2O_3 thin films. A pure Mott PM–PI phase transition at high temperatures (200 K–350 K) is indicated by the vertical continuous line. The shaded area indicates the intermediate phases accessible by strain engineering the in-plane lattice parameter. The green and yellow circles correspond to the low temperature transitions to the AFI phase in pure and 1.5% Cr– V_2O_3 thin films, respectively.

temperature in pure and 1.5% Cr-doped V_2O_3 thin films suggests that the first order Mott PM–PI transition line [dashed line in Fig. 4 (top)] in the bulk phase diagram should be replaced by two straight lines comprising a region of intermediate states between the stable PM and PI ones. These intermediate states are characterized by lattice parameter, RTR, and optical constant values between the bulk PM and PI ones. Although these results point to the stabilization of homogeneous intermediate states, local techniques will be

necessary to investigate whether there is phase coexistence at nanometric scales. These novel intermediate phases, accessible thanks to the systematic control of strain by heteroepitaxy, can be very interesting for applications based on V_2O_3 compounds. For example, the changes in resistivity vs lattice parameter could be exploited by inducing lattice deformations when applying an electric field to a nearby piezoelectric material²⁰ or by depositing the material on a membrane, and the effect can be used as a piezoresistive transduction mechanism.

The observation of a PM–PI phase transition by strain engineering in a wide range of temperatures (around room temperature) shows that the Mott transition can be solely driven by lattice deformation. In contrast, the temperature-driven transition to the AFI phase [yellow and green circles in Fig. 4 (bottom)] is preserved for the whole range of in-plane lattice parameters studied in this work.⁴⁷ Notably, the temperature dependence of the boundary between the PM (or PI) and AFI phases resembles the one for the bulk samples. The robustness of both PM–AFI and PI–AFI transitions against substrate clamping can be related to the considerably larger thermodynamic enthalpy of formation ($\Delta H = 2.03$ kJ/mol and 2.36 kJ/mol, respectively) as compared to the enthalpy of formation for the PM–PI ($\Delta H = 0.15$ kJ/mol) transition.^{48,49}

IV. CONCLUSION

In this work, the direct connection between the structure, electronic, and optical properties has been exploited to control the Mott MIT phase transition at room temperature in V_2O_3 thin film compounds. Intermediate states between PM and PI phases, which are not accessible in bulk, are realized by “smart” heteroepitaxy based on the fabrication of tailored artificial substrates. It is demonstrated that the Mott MIT can be induced at RT both, in pure and Cr-doped compounds, by strain engineering, leading to films with a colossal $\Delta R/R \sim 100\,000\%$ and a broad range of optical constants. These results demonstrate that Cr doping is actually not the key control parameter for the RT Mott MIT, in contrast to the observations in the bulk. Moreover, strain engineering leads to a more homogeneous modification of Mott materials compared to chemical doping, where the modification occurs locally on specific sites.

The observed unique electrical and optical properties are attributed to the strain-modulated bandgap beyond the bulk value of 0.1 eV. Our data suggest that the significant spectral weight at low energies in the bulk PI phase, traditionally considered as a hallmark of Mott physics,^{11–13,50} might not be an intrinsic feature but an artifact owing to local inhomogeneities. X-ray absorption and photo-emission spectroscopy studies together with theoretical calculations considering the lattice deformations and local structures could give more detailed insight into the changes in the electronic band structure and the origin of the modulated bandgap in the strained films.

Finally, the stabilization of a Mott PM–PI transition, in both pure and Cr-doped V_2O_3 thin films, around room temperature and the possibility to modify the structural, electrical, and optical properties in a continuous manner can be used in more practical concepts such as pressure sensors, resonators, acoustic light modulators, and photonic devices in the near-infrared range.

AUTHORS' CONTRIBUTIONS

P.H. performed all the MBE thin film growth experiments and the x-ray diffraction measurements and analysis. P.H. and M.M. performed the electrical measurements and analysis. J.W.S performed the TEM and EDX analysis. S.P. measured the SE spectra and fitted the data to extract the optical constants. P.H. performed the SE data analysis. J.-P.L. conceived the underlying concept and experiments. J.-P.L, P.H., M.M., and J. W. S. interpreted the data and wrote the final version. All authors contributed to the writing of the manuscript and the scientific understanding.

SUPPLEMENTARY MATERIAL

See the [supplementary material](#) for x-ray diffraction data of the Cr-doped V_2O_3 series, an example of the steps followed to fit the spectroscopic ellipsometry data, and the resulting optical constants of the Cr-doped V_2O_3 series in the energy range from 0.5 eV to 6 eV.

ACKNOWLEDGMENTS

The authors acknowledge financial support from the EU H2020 Project No. 688579 PHRESCO and the KU Leuven projects (Grant No. GOA/13/011, Fundamental challenges in Semiconductors, and Grant No. C14/17/080, 2D Oxides). J. W. S and J.-P. L. are also grateful to FWO (AKUL/13/19). We thank Dr. Ruben Lieten for the program to analyze reciprocal space maps data and Dr. Ilse Lenaerts for critical reading of the manuscript. P.H. acknowledges the support from Becas Chile—CONICYT.

DATA AVAILABILITY

The data that support the findings of this study are available from the corresponding authors upon reasonable request.

REFERENCES

- 1 D. B. McWhan, A. Menth, J. P. Remeika, W. F. Brinkman, and T. M. Rice, “Metal-insulator transitions in pure and doped V_2O_3 ,” *Phys. Rev. B* **7**, 1920–1931 (1973).
- 2 D. B. McWhan and J. P. Remeika, “Metal-insulator transition in $(V_{1-x}Cr_x)_2O_3$,” *Phys. Rev. B* **2**, 3734–3750 (1970).
- 3 D. B. McWhan, T. M. Rice, and J. P. Remeika, “Mott transition in Cr-doped V_2O_3 ,” *Phys. Rev. Lett.* **23**, 1384–1387 (1969).
- 4 B. A. Frandsen *et al.*, “Volume-wise destruction of the antiferromagnetic Mott insulating state through quantum tuning,” *Nat. Commun.* **7**, 12519 (2016).
- 5 P. D. Dernier and M. Marezio, “Crystal structure of the low-temperature antiferromagnetic phase of V_2O_3 ,” *Phys. Rev. B* **2**, 3771 (1970).
- 6 P. A. Metcalf *et al.*, “Electrical, structural, and optical properties of Cr-doped and non-stoichiometric V_2O_3 thin films,” *Thin Solid Films* **515**, 3421–3425 (2007).
- 7 S. Lupi *et al.*, “A microscopic view on the Mott transition in chromium-doped V_2O_3 ,” *Nat. Commun.* **1**, 105 (2010).
- 8 B. Mansart *et al.*, “Photoemission microscopy study of the two metal-insulator transitions in Cr-doped V_2O_3 ,” *Appl. Phys. Lett.* **100**, 014108 (2012).
- 9 F. Rodolakis *et al.*, “Inequivalent routes across the Mott transition in V_2O_3 explored by X-ray absorption,” *Phys. Rev. Lett.* **104**, 047401 (2010).
- 10 F. Rodolakis, “Evolution of the electronic structure of a Mott system across its phase diagram: X-ray absorption spectroscopy study of $(V_{1-x}Cr_x)_2O_3$,” *Phys. Rev. B* **84**, 245113 (2011).
- 11 P. Hansmann *et al.*, “Mott-Hubbard transition in V_2O_3 revisited,” *Phys. Status Solidi B* **250**, 1251–1264 (2013).
- 12 Y. Guo, S. J. Clark, and J. Robertson, “Calculation of metallic and insulating phases of V_2O_3 by hybrid density functionals,” *J. Chem. Phys.* **140**, 054702 (2014).

- ¹³D. N. Basov, R. D. Averitt, D. van der Marel, M. Dressel, and K. Haule, "Electrodynamics of correlated electron materials," *Rev. Mod. Phys.* **83**, 471 (2011).
- ¹⁴A. Ronchi *et al.*, "Early-stage dynamics of metallic droplets embedded in the nanotextured Mott insulating phase of V_2O_3 ," *Phys. Rev. B* **100**, 075111 (2019).
- ¹⁵M. Querré *et al.*, "Metal-insulator transitions in $(V_{1-x}Cr_x)_2O_3$ thin films deposited by reactive direct current magnetron co-sputtering," *Thin Solid Films* **617**, 56–62 (2016).
- ¹⁶P. Homm *et al.*, "Collapse of the low temperature insulating state in Cr-doped V_2O_3 thin films," *Appl. Phys. Lett.* **107**, 111904 (2015).
- ¹⁷N. B. Aetukuri *et al.*, "Control of the metal-insulator transition in vanadium dioxide by modifying orbital occupancy," *Nat. Phys.* **9**, 661 (2013).
- ¹⁸W. Liang *et al.*, "In-plane orientation-dependent metal-insulator transition in vanadium dioxide induced by sublattice strain engineering," *npj Quantum Mater.* **4**, 39 (2019).
- ¹⁹S. Autier-Laurent, B. Mercey, D. C. Chippaux, P. Limelette, and C. Simon, "Strain-induced pressure effect in pulsed laser deposited thin films of the strongly correlated oxide V_2O_3 ," *Phys. Rev. B* **74**, 195109 (2006).
- ²⁰P. Salev, J. del Valle, Y. Kalcheim, and I. K. Schuller, "Giant nonvolatile resistive switching in a Mott oxide and ferroelectric hybrid," *Proc. Natl. Acad. Sci. U. S. A.* **116**, 8798–8802 (2019).
- ²¹M. Querré *et al.*, "Non-volatile resistive switching in the Mott insulator $(V_{1-x}Cr_x)_2O_3$," *Physica B* **536**, 327–330 (2018).
- ²²N. Alyabyeva *et al.*, "Metal-insulator transition in V_2O_3 thin films caused by tip-induced strain," *Appl. Phys. Lett.* **113**, 241603 (2018).
- ²³E. B. Thorsteinsson, S. Shayestehaminzadeh, and U. B. Arnalds, "Tuning metal-insulator transitions in epitaxial V_2O_3 thin films," *Appl. Phys. Lett.* **112**, 161902 (2018).
- ²⁴L. Dillemans *et al.*, "Evidence of the metal-insulator transition in ultrathin unstrained V_2O_3 thin films," *Appl. Phys. Lett.* **104**, 071902 (2014).
- ²⁵H. Mashiko, T. Oshima, and A. Ohtomo, "Band-gap narrowing in α - $(Cr_xFe_{1-x})_2O_3$ solid-solution films," *Appl. Phys. Lett.* **99**, 241904 (2011).
- ²⁶H. Yang, R. J. Sladek, and H. R. Harrison, "Pressure dependence of elastic constants of $(V_{1-x}Cr_x)_2O_3$ at 296 K," *Phys. Rev. B* **31**, 5417 (1985).
- ²⁷H. Kuwamoto, J. M. Honig, and J. Appel, "Electrical properties of the $(V_{1-x}Cr_x)_2O_3$ system," *Phys. Rev. B* **22**, 2626 (1980).
- ²⁸S. E. Chamberlin *et al.*, "Optical absorption and spectral photoconductivity in α - $(Fe_{1-x}Cr_x)_2O_3$ solid-solution thin films," *J. Phys.: Condens. Matter* **25**, 392002 (2013).
- ²⁹L. Dillemans *et al.*, *Thin Solid Films* **520**, 4730 (2012).
- ³⁰J. Brockman *et al.*, *Appl. Phys. Lett.* **98**, 152105 (2011).
- ³¹W. R. Robinson, "High-temperature crystal chemistry of V_2O_3 and 1% chromium-doped V_2O_3 ," *Acta Crystallogr., Sect. B* **31**, 1153–1160 (1975).
- ³²J. Sakai *et al.*, "Strain-induced resistance change in V_2O_3 films on piezoelectric ceramic disks," *J. Appl. Phys.* **125**, 115102 (2019).
- ³³M. J. Rozenberg *et al.*, "Optical conductivity in Mott-Hubbard systems," *Phys. Rev. Lett.* **75**, 105 (1995).
- ³⁴I. Lo Vecchio *et al.*, "Optical properties of V_2O_3 in its whole phase diagram," *Phys. Rev. B* **91**, 155133 (2015).
- ³⁵A. S. Barker, Jr. and J. P. Remeika, "Optical properties of V_2O_3 doped with chromium," *Solid State Commun.* **8**, 1521–1524 (1970).
- ³⁶M. K. Stewart *et al.*, "Insulator-to-metal transition and correlated metallic state of V_2O_3 investigated by optical spectroscopy," *Phys. Rev. B* **85**, 205113 (2012).
- ³⁷L. Baldassarre *et al.*, "Quasiparticle evolution and pseudogap formation in V_2O_3 : An infrared spectroscopy study," *Phys. Rev. B* **77**, 113107 (2008).
- ³⁸M. M. Qazilbash *et al.*, "Mott transition in VO_2 revealed by infrared spectroscopy and nano-imaging," *Science* **318**, 1750–1753 (2007).
- ³⁹M. Brahlek *et al.*, "Opportunities in vanadium-based strongly correlated electron systems," *MRS Commun.* **7**, 27–52 (2017).
- ⁴⁰J. M. Tomczak and S. Biermann, "Multi-orbital effects in optical properties of vanadium sesquioxide," *J. Phys.: Condens. Matter* **21**, 064209 (2009).
- ⁴¹M. Fox, *Optical Properties of Solids* (Oxford University Press, 2001).
- ⁴²M. Eckstein, M. Kollar, and D. Vollhardt, "Isosbestic points in the spectral function of correlated electrons," *J. Low Temp. Phys.* **147**, 279–293 (2007).
- ⁴³W. W. Li *et al.*, "Intrinsic evolutions of optical functions, band gap, and higher-energy electronic transitions in VO_2 film near the metal-insulator transition region," *Appl. Phys. Lett.* **99**, 241903 (2011).
- ⁴⁴S.-K. Mo *et al.*, "Photoemission study of $(V_{1-x}M_x)_2O_3$ ($M = Cr, Ti$)," *Phys. Rev. B* **74**, 165101 (2006).
- ⁴⁵G. A. Thomas *et al.*, "Observation of the gap and kinetic energy in a correlated insulator," *Phys. Rev. Lett.* **73**, 1529 (1994).
- ⁴⁶J. B. K. Kana, J. M. Ndjaka, G. Vignaud, A. Gibaud, and M. Maaza, "Thermally tunable optical constants of vanadium dioxide thin films measured by spectroscopic ellipsometry," *Opt. Commun.* **284**, 807–812 (2011).
- ⁴⁷The transition temperature for the films with the largest in-plane lattice parameters were obtained from optical transmission measurements.
- ⁴⁸H. V. Keer, D. L. Dickerson, H. Kuwamoto, H. L. C. Barros, and J. M. Honig, "Heat capacity of pure and doped V_2O_3 single crystals," *J. Solid State Chem.* **19**, 95–102 (1976).
- ⁴⁹H. V. Keer, H. L. C. Barros, D. L. Dickerson, A. T. Barfknecht, and J. M. Honig, "Thermal studies on Cr-doped V_2O_3 crystals," *Mater. Res. Bull.* **12**, 137–143 (1977).
- ⁵⁰G. Kotliar, "The Mott transition in V_2O_3 and $NiSe_xS_{2-x}$: Insights from dynamical mean field theory," *Physica B* **259**, 711–714 (1999).
- ⁵¹G. E. Jellison, Jr. and F. A. Modine, "Parameterization of the optical functions of amorphous materials in the interband region," *Appl. Phys. Lett.* **69**, 371–373 (1996).